Optical Properties of Silver and Gold Tetrahedral Nanopyramid Arrays Prepared by Nanosphere Lithography

6 AUTHORS, INCLUDING:

Mohammadali Tabatabaei
The University of Western Ontario
15 PUBLICATIONS   **87** CITATIONS

SEE PROFILE

Alexandre Sangar
NawaTechnologies
9 PUBLICATIONS   **53** CITATIONS

SEE PROFILE

Philippe Torchio
Aix-Marseille Université
76 PUBLICATIONS   **822** CITATIONS

SEE PROFILE

Alexandre Merlen
Université de Toulon
36 PUBLICATIONS   **409** CITATIONS

SEE PROFILE

# Optical Properties of Silver and Gold Tetrahedral Nanopyramid Arrays Prepared by Nanosphere Lithography

Mohammadali Tabatabaei,[†,#] Alexandre Sangar,[‡,#] Nastaran Kazemi-Zanjani,[†,#] Philippe Torchio,[‡] Alexandre Merlen,*[,‡] and François Lagugné-Labarthet*[,†]

[†]Department of Chemistry and Centre for Advanced Materials and Biomaterials, University of Western Ontario, 1151 Richmond Street, London, Ontario, N6A 5B7, Canada

[‡]Institut des Matériaux et Nanomatériaux de Provence (UMR 7334), Université Aix-Marseille and Université du Sud Toulon Var, France

Ⓢ Supporting Information

ABSTRACT: Tetrahedral nanopyramids made of silver and gold over ITO/glass surfaces are fabricated. Our protocol is based on nanosphere lithography (NSL) with the deposition of thicker metal layers. After removing the microspheres used in the NSL process, an array of metallic tetrahedral nanostructures of ∼350−400 nm height is formed. The reported procedure avoids the use of any stabilizing surfactant molecules that are generally necessary to segregate the individual particles onto surfaces. We focus here on the optical and the physical properties of these plasmonic surfaces using near-field spectroscopy in conjunction with finite difference time domain (FDTD) modeling of the electric field. Remarkably, FDTD shows that the localized surface plasmon resonance is confined in the plane formed by the edges of two facing pyramids that is parallel to the polarization of the impinging excitation laser. The variable gap between the edges of two adjacent pyramids shows a broader localized surface plasmon and a larger specific surface as opposed to the usual nanotriangle array. Localized enhancement of the electric field is experimentally investigated by coating the plasmonic surface with a thin film of photosensitive azopolymer onto the surface of the nanopyramids. Upon irradiation, the deformation of the surface topography is visualized by atomic force microscopy and suggests the potentiality of these 3D nanopyramids for near-field enhancement. This last feature is clearly confirmed by surface-enhanced Raman scattering measurement with 4-nitrothiophenol molecules deposited on the pyramid platforms. The potentiality of such 3D nanostructures in plasmonics and surface spectroscopy is thus clearly demonstrated.
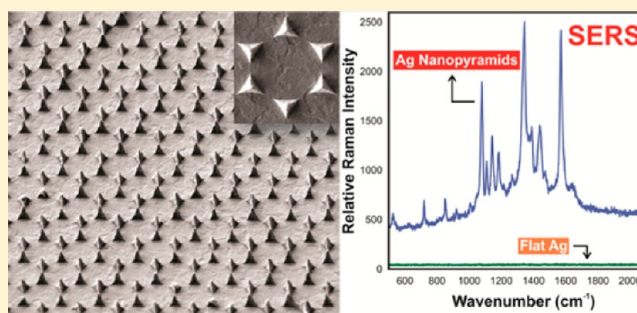
■ INTRODUCTION

Plasmonic structures produced by advanced nanofabrication techniques open up new possibilities when the manipulation of a resonant optical field is of interest.[1] The current advances in plasmonics technology for active and passive photonic devices,[2−4] spectroscopic applications,[5−7] and the conception of photovoltaic devices[8] all arise from the possibility to fabricate metallic nanostructures into a short-range arrangement over large surfaces. Electron-beam lithography[9,10] and focused ion beam are particularly well suited for the fabrication of high-resolution features (∼10 nm) on small areas. Other approaches using nanoimprint lithography[8,11] and deep-UV lithography followed by epitaxial growth or atomic layer deposition or annealing[8,12] are common techniques used to make plasmonic surfaces with features as small as 10 nm over standard 4, 6, and 12 in. wafers.

Among the available nanofabrication methods, nanosphere lithography (NSL) is a versatile and economical approach to make sharp nanostructures organized onto large surfaces.[13] These nanostructures have various applications ranging from surface-enhanced spectroscopy and surface plasmon resonance measurements for biosensing applications[14] to solar cell applications with the ultimate goal to improve the photovoltaic conversion efficiency.[15] Initially reported by Fischer and Zingsheim,[16] NSL platforms use the properties of the localized surface plasmon resonance (LSPR) confined at the apexes formed by two adjacent nanotriangles.[14,17−21] In NSL, a monolayer of silica or polystyrene nanoparticles is formed onto mica, silicon, or glass wafer.[22] A thin layer of silver or gold with a thickness of around 30 nm is then deposited on this monolayer. Once the particles are removed, an array of metallic nanotriangles (Au, Ag) of 20−30 nm thicknesses is formed over the substrate. However, in most cases, only a thin layer of metal is deposited leading to simple flat triangles array.

In this work, we show that the deposition of a thicker layer of metal with thickness of roughly half of the diameter of an

individual particle leads to the formation of tetrahedral pyramids organized in a hexagonal pattern. Herein, we mainly focus our study on optical near-field and plasmonics properties of such nano-objects. Noteworthy, the proposed protocol can be used for a variety of other applications by changing the composition of deposited material. Such 3D and sharp nanopyramids could be used for hydrophobic surfaces, field emission, catalysis, and many other applications.[13] Furthermore, these 3D individual objects can be further functionalized with guest molecules and can be used as the platform for enhanced optical sensing. The optical properties of these arrays were first investigated using FDTD calculations for Ag and Au nanostructures along the transverse and longitudinal planes with respect to the polarization direction of 532 and 632.8 nm excitation wavelengths. To visualize the areas with maximum field enhancement, we used the approach developed by Hubert and co-workers[23−25] using a thin film of a photosensitive azobenzene polymer and compared the topographical changes probed by atomic force microscopy (AFM) to the numerical calculations of the electric field.

Finally, the Raman surface enhancements of these platforms are systematically investigated for gold and silver nanopyramids at both 532 and 632.8 nm excitations. Silver nanopyramids demonstrated the highest enhancement of the Raman signal leading to the photochemical transformation of 4-nitro-thiophenol (NTP). Photogeneration of dimercaptoazobenzene appears to be effective for both excitation wavelengths, although 532 nm is always more efficient even under modest irradiation of 200 μW.

■ EXPERIMENTAL SECTION

Materials. Microscope coverslips (22 × 22 × 0.15 mm) were purchased from VWR International, Mississauga, Canada. Nochromix was purchased from Godax Laboratories Inc., Maryland, United States. Hydrogen peroxide (30% v/v) was obtained from EMD Inc., Mississauga, Canada. Polystyrene microspheres (10% w/w) of 1 μm diameter were purchased from ThermoScientific Co (California, United States). Sodium dodecyl sulfate (SDS) was obtained from Sigma-Aldrich, Missouri, United States. Glass slides coated with 110 nm indium thin oxide (ITO) were purchased from Lumtec (Taiwan).

Preparation of Samples by Nanosphere Lithography (NSL). A detailed description of the preparation of the samples can be found elsewhere.[26,17] Briefly, microscope coverslips used to prepare the monolayer of polystyrene particles at the water surface were first sonicated in acetone for 5 min followed by cleaning in nochromix solution in concentrated sulphuric acid for 15 min. Subsequently, the slides were rinsed in Milli-Q ultrapure water (18.2 MΩ·cm) several times. These were sonicated for 1 h in a mixture of ammonium hydroxide:hydrogen peroxide:ultrapure water (18.2 MΩ·cm) in a ratio of 5:1:1. Afterward, the glass slides were sonicated for 15 min in water. Polystyrene microspheres solution was equilibrated to room temperature prior to use. Thereafter, a 30 μL aliquot of polystyrene solution was mixed with 30 μL of ethanol (100%). Twenty microliters of the prepared solution was deposited on top of the dried coverslip. This was immediately introduced in the air−water interface of a 6 cm Petri dish filled with ultrapure water (18.2 MΩ·cm). The coverslip floated on the air−water interface, and the polystyrene colloidal solution spread out to the air−water interface. After the dispersion of the solution, the coverslip sank to the bottom of the Petri dish. A few drops of

2% (w/v) SDS solution in water were added to further group the nanospheres into an ordered monolayer. The nanosphere solution was finally picked up using a wet and clean glass slide coated with ITO and was allowed to dry overnight under a Petri dish.

Metal Deposition and Characterization. After the samples were dried, 350−400 nm of Au was deposited using electron beam evaporation (Hoser, Ottawa, Canada). The polystyrene particles were finally removed by sonicating the sample in ethanol for about a minute. The sample was then dried under the nitrogen gas. Scanning electron microscope (SEM) images were obtained using a LEO Zeiss 1540XB (Zeiss, Oberkochen, Germany). Atomic force microscopy measurements were performed with a NanoWizard II bioscience from JPK instruments (Berlin, Germany). AFM scans were conducted in noncontact mode using standard AFM tips (NCL20 Nano World Inc.: resonance frequency f = 170 kHz, force constant k = 48 N/m or NSC15/AlBS Micromash: resonance frequency f = 325 kHz, force constant k = 46 N/m).

FDTD Simulations. The distribution of the electric field intensity in close proximity of the silver and gold nanopyramids was calculated using FDTD Solutions (Lumerical Solutions, Inc.). The calculations were set up as a three-dimensional system with a 0.15 nm resolution grid, for 1000 fs, including appropriate boundary conditions. A plane wave source was chosen at 532 or 632.8 nm working wavelengths with a propagation axis perpendicular to the plane of the single or lattice of pyramids and with a polarization along the X axis. The physical parameters, such as size and height of the nanopyramids, used in these calculations were obtained from the AFM and SEM data. The dielectric constants of the ITO, glass (silicon dioxide), silver, and gold were described by the Drude model provided in the material database from the software. The calculation of the relative total electric field intensity ($|E|^2$) and its image plot was obtained from the contribution of its components ($|E_x|^2 + |E_y|^2 + |E_z|^2$), and it was calculated at the apex or the bottom of the pyramids.

Azopolymer Thin Film Preparation and Photoinduced Surface Deformation. A solution of poly{4′-[[[[(methacryloyloxy)ethyl]ethyl]amino]-4-nitroazobenzene-co-methyl methacrylate} with 11% molar azobenzene moieties (p(DR1M-co-MMA)-11%) was prepared in chloroform (0.05 g in 5 mL of solvent) and was spin-casted over the nanopyramids at a speed of 1000 rpm. The films were annealed 10 min at 100 °C. Resulting film thickness was of 80 nm as measured by atomic force microscopy on a small scratch made with the tip of a needle. To induce azobenzene surface deformation, irradiation was conducted at 532 nm (Coherent, Compass 315 M Laser) with an expanded beam of about 6 mm, and an irradiance was set to 100 mW/cm^2 for an irradiation time of 15 min.

Raman SERS Measurements. The Raman measurements were performed using a Horiba Jobin-Yvon Raman spectrometer equipped with a 600 grooves/mm grating and a 532 or 632.8 nm excitation with proper interference and edge filters. For both laser sources, intensities were set to 2 mW or 200 μW at the sample using neutral density filters with 1.0 or 2.0 optical densities, respectively. Microscope objective of 40×, 0.7 N.A. was used for all experiments. The pinhole of the spectrometer was opened to 300 μm. All Raman spectra are shown without baseline correction.
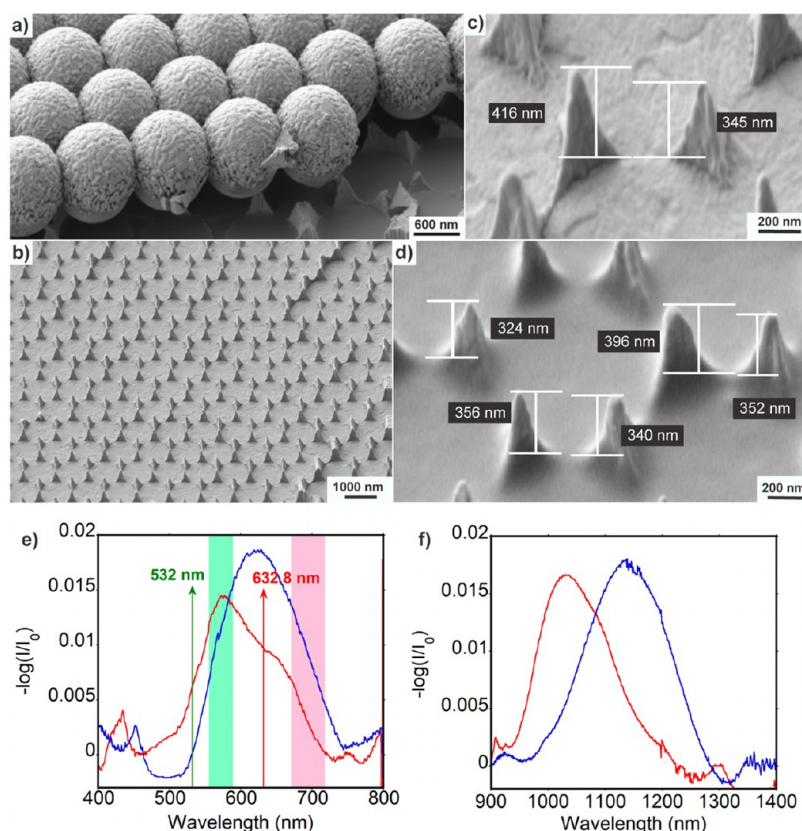
Figure 1. (a) SEM images of silver-coated polystyrene nanospheres. (b) Array of silver nanopyramids. (c, d) Individual silver nanopyramids before and after coating with an azopolymer thin film, respectively. (e, f) Extinction spectra of the silver (red) and gold (blue) nanopyramids. Excitation wavelengths as well as the spectral ranges between 800 and 1800 cm^{-1} with respect to both excitations are indicated.

■ RESULT AND DISCUSSIONS

A variety of methods have been reported for the fabrication of organized arrays of sharp nanotip structures for SERS applications. Conical[27] or pyramidal[28−30] structures have been made using top-down approaches with the desire to obtain a very sharp apex at the extremity of the pyramids leading to efficient SERS platforms. It is noteworthy that these sharp nanostructures are often distant by several micrometers from each other.[31] Other bottom-up approaches have also been reported with the intention to obtain sharp tips. However, because of the inhomogeneous distribution of such structures over a surface, their application for analytical purposes such as SERS is compromised.[31,32] In the present work, it is shown that the sharpness of the tip is not the dominant effect for the enhancement. The proximity of the pyramids' edges is a much more important factor in particular when the irradiation source is polarized in the transverse direction with respect to the tip orientation. Inverted pyramids engraved on silicon and coated with gold that are commercially available for SERS measurements (Klarite TM, Renishaw diagnostic)[33] use the variable gaps between two opposed edges of the inverted pyramid. However, since they are opaque, they can be used only in reflection geometry. On the contrary, our structures can be used for both reflection/transmission measurements since the pyramids are deposited on a transparent ITO-coated glass substrate.

Characterization of Nanopyramid Arrays Fabricated by NSL. The resulting scanning electron microscopy (SEM) images of the nanopyramids formed by NSL are shown in Figure 1a−d after deposition of 400 nm layer of silver over the

1 μm diameter polystyrene spheres by electron-beam evaporation.

The principle of NSL is depicted in the Supporting Information (Figure S1, Supporting Information (SI)). The triangular voids between three adjacent spheres in close contact get smaller during the deposition process leading to the formation of pyramidal structures. The indium tin oxide (ITO) layer of 120 nm thickness over the glass slide forms an adhesive layer avoiding further deposition of chromium or titanium deposition. It can be clearly seen that both deposited metal and the ITO layer demonstrated intrinsic roughness on the substrate (Figure 1a). Subsequent to the lift-off process of the polystyrene nanoparticles, a large surface (mm^2) of homogeneous pyramids can be observed over the ITO substrate (Figure 1b). Similar structures have been obtained for gold (Figure S2, SI). The extinction spectra of both silver and gold nanopyramid arrays (Figure 1e, f) show two resonances corresponding to the quadrupolar and the dipolar contributions, respectively. For silver, the quadrupolar LSPR is expected at 550 nm, while for gold, this resonance is red-shifted to 585 nm. The dipolar contributions are even further shifted in the near-infrared range at 1035 and 1100 nm, respectively.

Finite Difference Time Domain (FDTD) Calculations. To estimate the influence of the geometry on the localization of the LSPR, we have performed a series of FDTD calculations for Au and Ag nanopyramids irradiated with 532 and 632.8 nm wavelengths. The results of the normalized intensity enhancement $|E/E_0|^2$ depicted in logarithm scale are shown in Figure 2 for Ag/532 nm, while other cases (Ag/632.8, Au/632.8, and
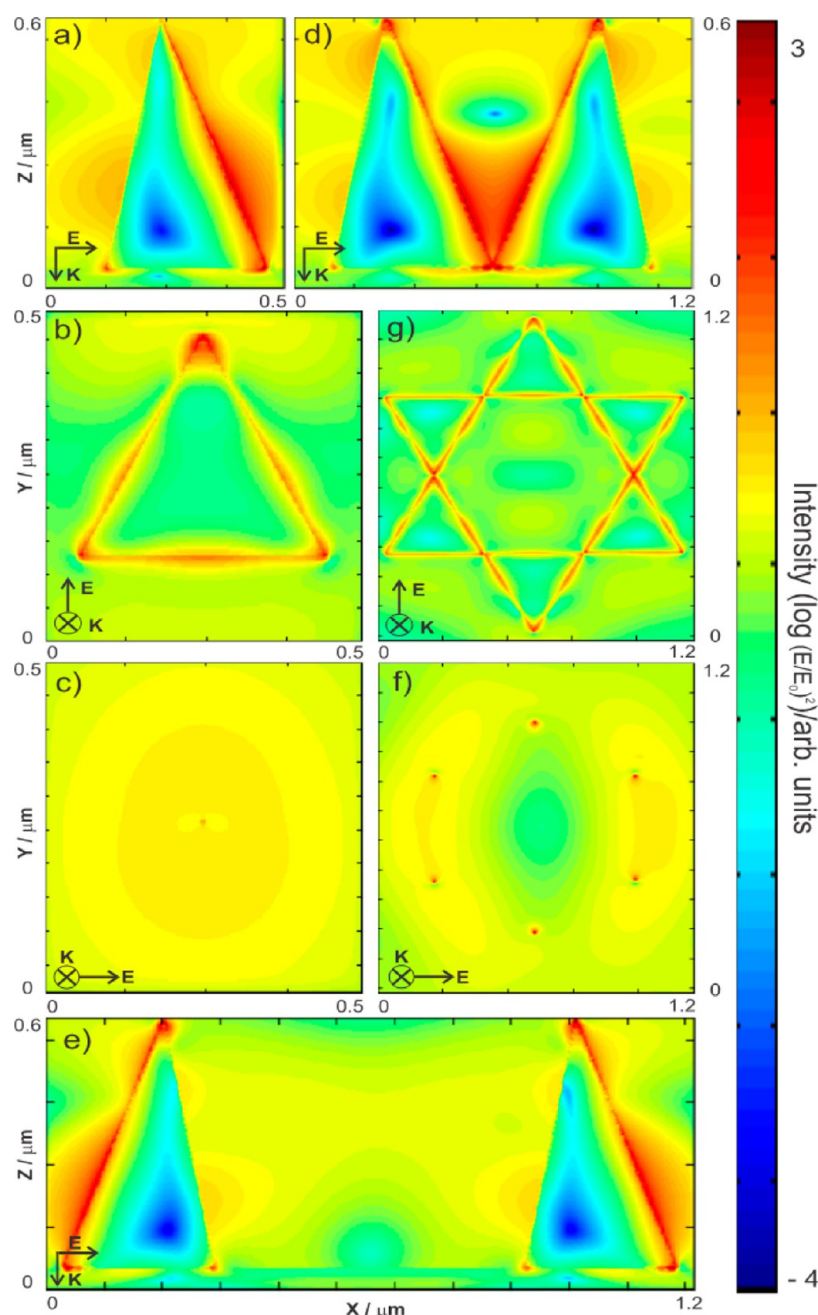
Figure 2. FDTD calculation of the transverse (b, c, f, g) and longitudinal (a, d, e) components of the electric field ($|E/E_0|^2$, log scale representation) for silver nanopyramids prepared on ITO and irradiated at 532 nm. The transverse fields shown in (c, f) are calculated 2 nm above the tips of the pyramids. The transverse fields shown in (b, g) are calculated 2 nm above the ITO base layer.

Au/532) are provided in the Supporting Information (Figures S3−S5).

In Figure 2a−c, a single isolated pyramid was also investigated. The EM field was calculated in both longitudinal and transverse directions as shown in Figure 2a−c. In Figure 2a, the field is significantly confined along the edge of the pyramids, which is also oriented along the polarization direction.

The typical field enhancement shown in log scale corresponds to 20 fold enhancement of the electric field approximately. The field was calculated in the transverse plane with respect to light propagation 2 nm above the base of the pyramid (Figure 2b) and 2 nm above the summit of the pyramid (Figure 2c). Localized enhancement can be clearly

seen at the three base corners of the pyramids (intensity enhancement of $|E/E_0|^2 = 10^3$), while the enhancement at the summits of the pyramid is limited (intensity enhancement of $10^{1.68} \sim 50$). This indicates that the polarization of the input light must have a component along the tip axis and no component in the orthogonal direction. Such observation was reported for nanoscale resolution tip-enhanced Raman spectroscopy (TERS), where the impinging field was ideally polarized along the tip axis to excite the plasmon modes resonance of the metalized tip. This was then employed as a local nanoantennae to probe the surface of interest.[34,35]

Further modeling was conducted on an array of pyramids arranged in a hexagonal lattice along the longitudinal and transverse planes with respect to the propagation direction **k**. In

Figure 2d, the field in the longitudinal plane of two facing pyramids was investigated. In this case, the field was also considerably confined along the facing edges of the pair of pyramids that formed variable gaps.

Typically, the field is confined from the base of the pyramids to about half the height of the pyramids' summit. This is also observed for other material/wavelength configurations such as Ag/632.8 (Figure S3-d, SI) and Au/632.8 (Figure S4-d, SI) as opposed to Au/532 (Figure S5-d, SI). In the latter configuration, the field enhancement was confined along the edges of the pyramid pairs. However, no effective coupling was observed between the facing pyramids. The results clearly showed that the variable gap between opposed pyramids can be beneficial to applications in plasmon-enhanced spectroscopy because the matching between the plasmon resonance frequency and the excitation light frequency may not be critical. In other words, from calculations shown in Figure 2 and Figure S3 (SI), silver nanopyramids are expected to be efficient for field enhancement at both 532 and 632.8 nm wavelengths. For gold pyramids, the scenario is different, and coupling was mainly effective when 632.8 nm excitation was being used. As shown in Figures S3d and S4d (SI), coupling between facing pyramids was only observed at 632.8 nm, while for 532 nm the enhanced field was mainly observed along the opposed edges of the nanopyramids but without any coupling. On the basis of these calculations, we can then expect a much lower overall enhancement for gold pyramids exposed by 532 nm wavelengths, while silver pyramids will be effective for both wavelengths. For surface-enhanced Raman, this is of interest, but one must consider as well the enhancement of the Raman shifted frequencies. As shown in Figure 1e, ideally, both $E_{excitation}$ and E_{Raman} must be in resonance or preresonance with the extinction of the plasmon frequency to be enhanced. When these two conditions are fulfilled, the electromagnetic enhancement, F, is given by[36]

$$F = \left| \frac{E_{excitation}}{E_0} \right|^2 \left| \frac{E_{Raman}}{E_0} \right|^2 \qquad (1)$$

It appears that excitations at 532 and 632.8 nm are both resonant for the silver nanostructure, which gave rise to the enhancement of the Raman signal in the fingerprint region of the molecule of interest. From the FDTD calculation, assuming an intensity enhancement of 10^3 at both the excitation and the Raman wavelengths for Ag/532 nm, eq 1 yields to an overall SERS enhancement factor of $\sim 10^6$ which is comparable to reported values in literature.[10] However, for gold pyramids, since the excitation of 532 nm is weakly resonant with the quadrupolar contribution of pyramidal structure, a smaller Raman enhancement is therefore expected.

Mapping Individual Hot-Spots on Photosensitive Self-Developing Azopolymer. To visualize the confinement of the field over the whole plasmonic structure, experiments using a photosensitive polymer were conducted on the nanostructures. An azobenzene thin layer (80 nm) was spin coated over the whole silver nanopyramid arrays leading to a smooth surface as shown in Figure 1d. Azobenzene polymer is of particular interest because it undergoes surface migration and subsequent topographical changes upon irradiation by resonant light. In this study, we used p(DR1M-co-MMA) with a molar ratio in azobenzene moieties of 11% (Scheme 1). The donor (NH_2) and acceptor (NO_2) groups located on opposite sides of the azobenzene core are responsible for the large charge density

Scheme 1. Chemical Structure of p(DR1M-co-MMA) 11%
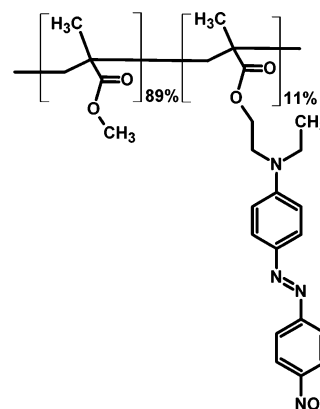
on the molecule leading to a colorful thin film material with an absorption at maximum wavelength of $\lambda = 500$ nm and an extinction coefficient of $\varepsilon = 70\,000$ l·mol^{-1}·cm^{-1}. Therefore, an excitation wavelength of 532 nm will be doubly resonant with (1) the plasmon resonance of the silver pyramids array and (2) the absorption of the azobenzene polymer leading to the most efficient surface deformation. Atomic force microscopy images were collected on the samples before and after irradiation at 532 nm with an irradiance of 100 mW/cm^2 (Figure 3a, b). Subtle changes in the surface topography can be observed after irradiation for 15 min as shown by the indicated cross sections 1 and 2 on the AFM images. A topographical increase of 7 ± 2 nm can also be systematically measured at the center of a lattice (cross section 1) over several individual lattices as shown in Figure 3b, d. The cross section shown in Figure 3d shows a bimodal increase with two maxima separated by a smaller minimum. This change of topography is a very useful indicator of the field location knowing that azopolymers migrate from areas where the field is large toward areas where the field is weaker. As shown in Figure 2g for silver pyramids, the field calculated 2 nm above the pyramid base is indeed weaker at the center of the lattice, while the most intense field was observed at the apexes between facing triangles.

The azopolymer molecules migrated toward the center of the lattice as expected. The small minimum between the two maxima can be explained by the competition between the migration processes coming from both sides. A similar effect has been reported previously for studies where gratings were inscribed holographically onto thin films of azopolymers leading to half periodic structures with respect to the interference fringe spacing.[37] This is the result of photodriven mass transport from successive photoisomerization steps.[38,39] This photoinduced mechanism suggests possible strong alterations of the local viscoelastic properties of the polymer and changes of the local densities that further alter the migration of the polymer chains toward the center of the lattice.[37] Similar changes were obtained when the cross section was measured along closely facing triangles (cross section 2 on the AFM images). As shown in Figure 3e, f, the topographical change is small. It is less than 5 nm in height variation but is yet very clearly observable by AFM. Also, the change of the slopes along the edges of two facing pyramids is due to the migration of the photosensitive polymer mediated and amplified by the plasmonic resonance. The slope of the polymer thin film deposited over the pyramids becomes steeper after irradiation, which indicates a mass flow from the area where enhancement
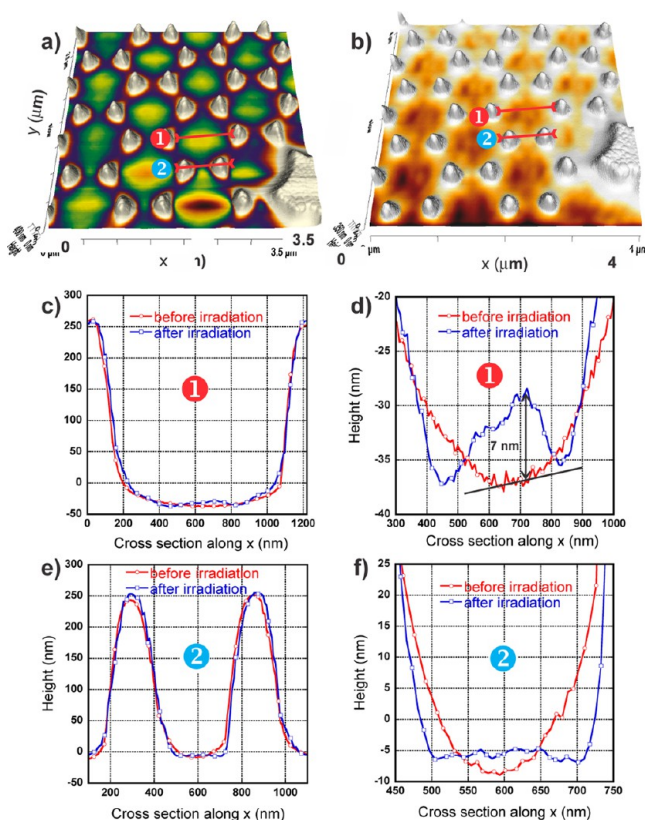
Figure 3. (a, b) AFM images of Ag nanopyramids prepared on ITO coated with a 80 nm azopolymer thin film layer (a) before and (b) after 15 min of irradiation with an irradiance of 100 mW/cm². (c, d) Topographical cross sections along the center of a hexagonal lattice (1) of Ag nanopyramids before and after irradiation. The height scale of d has been expanded to show better the small topographical changes occurring at the center of the lattice. (e, f) AFM topographical cross sections along the closest facing silver pyramids (2) before and after irradiation. The height scale of f has been expanded to show better the small topographical changes occurring at the center of the lattice and the edges of the pyramids.

of the field is high, because of the plasmon enhancement, toward regions where the field is weaker. In addition, the gap between the two facing pyramids indicates a weaker field enhancement at the exact center between the facing pyramids. Thus, the polymer migration is predominantly observed along the edge of the pyramids.

SERS Measurements. The capability of these pyramidal structures was further investigated for SERS application using a standard molecule. To perform this, the structures were immersed in a 1 mM solution of 4-nitrothiophenol (NTP) for 24 h and were subsequently rinsed with ethanol to remove nonadsorbed species.

Both gold and silver pyramid arrays were investigated with excitation wavelengths of 532 and 632.8 nm. The Raman spectra measured on the pyramidal nanostructures are reported in Figure 4 together with the reference spectra performed on the flat portion of the deposited metal. None of the reference spectra measured on flat gold and silver areas showed a spectral feature emphasizing the interest of using the nanostructured surface for the study of adsorbed monolayers.

We also compared side-by-side the SERS spectra from gold nanopyramids and nanotriangles made by NSL (Figure S6, SI). In the latter case (nanotriangles), the thickness of gold was 30
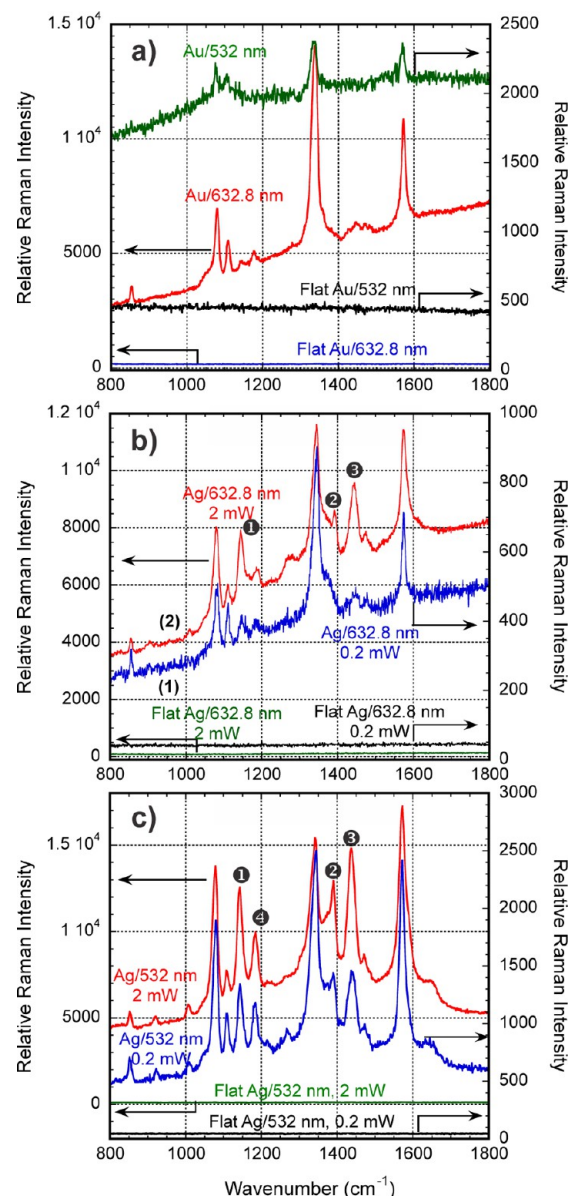

Figure 4. Raman spectra of NTP adsorbed on the nanopyramid arrays. The spectra were recorded with the same acquisition time (10 s). No baseline correction was performed. Raman spectra acquired on flat metal portions (no structures) and functionalized at the same conditions as shown. (a) SERS spectra collected on Au nanopyramids with 632.8 and 532 nm irradiations. (b) SERS spectra collected on Ag nanopyramids with 632.8 nm excitation under 0.2 mW (initial) and 2 mW (final) irradiations. (c) SERS spectra collected on Ag nanopyramids with 532 nm excitation under 0.2 mW and 2 mW irradiations. (d) SERS spectra recorded at 632.8 nm on Ag nanopyramids at 2 mW (initial) and 0.2 mW (final).

nm. At 632.8 nm excitation, the SERS spectra were systematically more intense for the nanopyramids as compared to the nanotriangles by a typical factor of ~4. This gain confirms the interest of the nanopyramids compared to the nanotriangles for ultrasensitive measurements.

The spectra shown in Figure 4a demonstrate an intense signal for gold pyramids upon irradiation at 632.8 nm, whereas the Raman spectrum is weak for 532 nm. This confirms that the matching between the excitation wavelength and the plasmon resonance is critical and was fulfilled only for the Au/632.8

case. The main spectral features observed in Figure 4a at 1078, 1107, 1340, and 1572 cm^{-1} are assigned to ν_{7a} (coupled with C–S bond), $\nu_{\phi-N}$, ν_s NO$_2$, and ν_{8b} of the phenyl group, respectively.[40] The SERS spectra of silver nanopyramids irradiated by 632.8 nm laser with 0.2 and 2 mW intensities are shown in Figure 4b. Noticeably, the initial spectrum recorded with 0.2 mW was similar to the Au/632.8 case in terms of relative intensities and magnitude. Silver pyramidal nanostructures have therefore a plasmon that can be used in conjunction with both irradiation wavelengths because, as shown in Figure 1e, both 532 and 632.8 nm wavelengths are preresonant with the plasmon absorption.

Considerably, the initial spectrum recorded with 0.2 mW was also similar to the Au/632.8 case in terms of relative intensities. However, when the laser power was increased to 2 mW, the collected spectra showed significant changes. This could be understood by considering the fact that 2 mW laser focused with high N.A. microscope objective implies a typical irradiance in the MW/cm^2 range. New bands at 1142, 1387, and 1437 cm^{-1} (noted 1, 2, and 3 in Figure 4b) were assigned to β_{C-H}, $\nu_{N=N} + \nu_{C=C} + \nu_{C-H}$, and $\nu_{N=N} + \nu_{C=C} + \beta_{C-H}$, respectively, while the intensity of the 1340 cm^{-1} band (ν_s NO$_2$) was decreased. Such observations were investigated by several groups and were assigned to photoinduced reduction of p-NTP on Ag surfaces to form dimercaptoazobenzene (DMAB).[40−42] More recently, time-resolved measurements using tip-enhanced spectroscopy were reported using a silver-coated AFM tip irradiated by a 532 nm excitation laser. Nonetheless, a nonresonant laser at 632.8 nm was used to probe the photoreduction as a function of irradiation time.[43]

Our results indicated that for these particular plasmonic platforms, even 632.8 nm can trigger the photoreduction of p-NTP into DMAB as long as irradiation intensity is sufficiently high. The same condition was also applied to silver structures at 532 nm, which exhibited the highest enhancement as shown in Figure 4c. For both intensities of the excitation source, the spectra showed the new peaks assigned to the formation of DMAB as in the case of Ag/632.8. However, the peak associated with the symmetric stretching mode of NO$_2$ was even further reduced in intensity indicating a higher photo-reduction yield upon 532 nm irradiation. Similarly, the Raman band at 1183 cm^{-1} (noted 4) in Figure 4c was significantly increased which has not been addressed in other studies. This clearly indicates that Ag/532 offered the highest enhancement conditions even at low power.

Significant relative intensity changes indicated the photo-induced transformation of the molecule of interest. Thus, a control experiment was performed to confirm the irreversibility of the photoinduced transformation. Using Ag/632.8 conditions, the intensity of 2 mW was first used to collect the first spectrum shown in Figure 5 (noted 1). The second spectrum (noted 2) in Figure 5 was collected after irradiation with 0.2 mW similar to the conditions of Figure 4b. In such a sequence, the spectral features recorded with the lowest intensity were identical to the spectra measured with higher intensity confirming the irreversibility of the photoinduced reaction.

■ CONCLUSION

In this work, we have prepared arrays of metallic nanopyramids made of gold and silver using nanosphere lithography. This study is focused on plasmonics properties and near-field enhancement of such a real 3D nanostructure. Both platforms
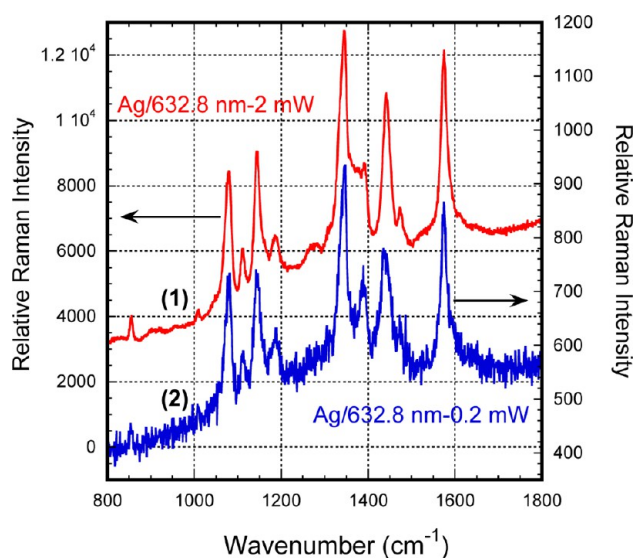

Figure 5. SERS spectra of NTP adsorbed onto silver nanopyramids recorded initially under 2 mW irradiance followed by a measurement under 0.2 mW with identical acquisition time (10 s).

were investigated upon irradiation by 532 and 632.8 nm wavelengths because the quadrupolar plasmon resonances of both structured metals have resonance close to these wavelengths. FDTD calculations in the transverse and longitudinal planes with respect to the propagation direction of the excitation source were systematically conducted for the four cases, namely, Au/532, Au/632.8 and Ag/532, Ag/632.8. These calculations clearly showed that the silver nanostructure can efficiently be excited at 532 and 632.8 nm, whereas gold nanostructure is not expected to be efficient at 532 nm. To complement these FDTD simulations, AFM characterization and Raman measurements were also conducted on the samples using photosensitive azopolymer thin film. This allows one to monitor topographical changes on the surface of silver nanostructure coated with a photoresponsive film. In addition, this opens up the opportunity to indirectly locate the area of high-field enhancement over the substrate. Finally, these structures were tested for SERS measurements with p-NTP molecules. As a result, SERS was observed predominantly for Ag/532, Ag/632.8, and Au/632.8. For silver nanostructures, photoreduction of p-NTP to DMAB was also observed. In the case of 632.8 nm irradiation, it was shown to be dependent on the laser intensity. Such changes were irreversible emphasizing the interest of metallic plasmonic platforms not only for surface enhancement but also for photoinduced chemical reaction at a monolayer of a material on the surface. These nanopyramid arrays fabricated on a conductive and transparent substrate can be further integrated in solar cells benefiting from both the plasmon enhancement of the solar spectrum and the electronic conduction of the ITO layer yielding to a higher photovoltaic conversion efficiency.

Beyond optical applications, we suggest that these high aspect ratio structures have also potential as superhydrophobic surfaces and field emission antennae. The extremely simple but efficient protocol proposed here on the basis of the well-known NSL lithography can be applied to many materials for the preparation of real 3D sharp nanopyramid arrays on large surfaces.

■ ASSOCIATED CONTENT

Ⓢ Supporting Information

Principle of nanosphere lithography, array of gold nanopyramids, FDTD calculations of the electric field for silver and gold nanopyramids, and Raman spectra of Au nanopyramids and Au nanotriangles. This material is available free of charge via the Internet at http://pubs.acs.org.

■ AUTHOR INFORMATION

Corresponding Author

*E-mail: flagugne@uwo.ca (F.L.-L.); merlen@univ-tln.fr (A.M).

Author Contributions

#These authors contributed equally.

Notes

The authors declare no competing financial interest.

■ ACKNOWLEDGMENTS

■ REFERENCES

(1) Brongersma, M. S.; Shalaev, V. M. The Case for Plasmonics. *Science* **2010**, *328*, 440−441.

(2) Krasavin, A. V.; Zayats, A. V. Electro-Optic Switching Element for Dielectric-Loaded Surface Plasmon Polariton Waveguides. *Appl. Phys. Lett.* **2010**, *97*, 041107−041110.

(3) Krasavin, A. V.; Zayats, A. V. Guiding Light at the Nanoscale: Numerical Optimization of Ultrasubwavelength Metallic Wire Plasmonic Waveguides. *Opt. Lett.* **2011**, *36*, 3127−3129.

(4) Aydin, K.; Ferry, V. E.; Briggs, R. M.; Atwater, H. A. Broadband Polarization-Independent Resonant Light Absorption Using Ultrathin Plasmonic Super Absorbers. *Nat. Commun.* **2011**, *2*, 1−7.

(5) Brolo, A. G. Plasmonics for Future Biosensors. *Nat. Photonics* **2012**, *6*, 709−713.

(6) Ahmed, A.; Gordon, R. Single Molecule Directivity Enhanced Raman Scattering using Nanoantennas. *Nano Lett.* **2012**, *12*, 2625−2630.

(7) Asiala, S. M.; Schultz, Z. D. Characterization of Hotspots in a Highly Enhancing SERS Substrate. *Analyst* **2011**, *136*, 4472−4479.

(8) Atwater, H. A.; Polman, A. Plasmonics for Improved Photovoltaic Devices. *Nat. Mater.* **2010**, *9*, 205−213.

(9) Yokota, Y.; Ueno, K.; Misawa, H. Highly Controlled Surface-Enhanced Raman Scattering Chips Using Nanoengineered Gold Blocks. *Small* **2011**, *7*, 252−258.

(10) Marquestaut, N.; Martin, A.; Talaga, D.; Servant, L.; Ravaine, S.; Reculusa, S.; Bassani, D. M.; Gillies, E.; Lagugné-Labarthet, F. Raman Enhancement of Azobenzene Monolayers on Substrates Prepared by Langmuir-Blodgett Deposition and Electron-Beam Lithography Techniques. *Langmuir* **2008**, *24*, 11313−11321.

(11) Li, K.; Clime, L.; Cui, B.; Veres, T. Surface Enhanced Raman Scattering on Long-Range Ordered Noble-Metal Nanocrescent Arrays. *Nanotechnology* **2008**, *19*, 145305.

(12) Dhawan, A.; Du, Y.; Batchelor, D.; Wang, D.; Leonard, D.; Misra, V.; Ozturk, M.; Gerhold, M. D.; Vo-Dinh, T. Hybrid Top-Down and Bottom-Up Fabrication Approach for Wafer-Scale Plasmonic Nanoplatforms. *Small* **2011**, *7*, 727−731.

(13) Ye, X.; Qi, L. Two-Dimensionally Patterned Nanostructures Based on Monolayer Colloidal Crystals: Controllable Fabrication, Assembly, and Applications. *Nano Today* **2011**, *6*, 608−631.

(14) Correia-Ledo, D.; Gibson, K.; Dhawan, A.; Couture, M.; Graham, D.; Vo-Dinh, T.; Masson, J. F. Assessing the Location of Surface Plasmons Over Nanotriangle and Nanohole Arrays of Different Size and Periodicity. *J. Phys. Chem. C* **2012**, *116*, 6884−6892.

(15) Abass, A.; Shen, H.; Bienstman, P.; Maes, B. Angle Insensitive Enhancement of Organic Solar Cells Using Metallic Gratings. *J. Appl. Phys.* **2011**, *109*, 023111.

(16) Fischer, U. C.; Zingsheim, H. P. Submicroscopic Pattern Replication with Visible Light. *J. Vac. Sci. Technol.* **1981**, *19*, 881−885.

(17) Huang, W.; Qian, W.; El-Sayed, M. A.; Ding, Y.; Wang, Z. L. Effect of the Lattice Crystallinity on the Electron-Phonon Relaxation Rates in Gold Nanoparticles. *J. Phys. Chem. C* **2007**, *111*, 10751−10757.

(18) Haynes, C. L.; Van Duyne, R. P. Plasmon-Sampled Surface-Enhanced Raman Excitation Spectroscopy. *J Phys. Chem. B* **2003**, *107*, 7426−7433.

(19) Huang, W.; Qian, W.; El-Sayed, M. A. Coherent Vibrational Oscillation in Gold Prismatic Monolayer Periodic Nanoparticle Arrays. *Nano Lett.* **2004**, *4*, 1741−1747.

(20) Morarescu, R.; Shen, H.; Vallée, R. A. L.; Maes, B.; Kolaric, B.; Damman, P. Exploiting the Localized Surface Plasmon Modes in Gold Triangular Nanoparticles for Sensing Applications. *J. Mater. Chem.* **2012**, *22*, 11537−11542.

(21) Fayyaz, S.; Tabatabaei, M.; Hou, R.; Lagugné-Labarthet, F. Surface-Enhanced Fluorescence: Mapping Individual Hot Spots in Silica-Protected 2D Gold Nanotriangle Arrays. *J. Phys Chem. C* **2012**, *27*, 1494−1498.

(22) Lenzmann, F.; Li, K.; Kitai, A. H.; Stöver, H. D. H. Thin-Film Micropatterning Using Polymer Microsphere. *Chem. Mater.* **1994**, *6*, 156−159.

(23) Hubert, C.; Rumyantseva, A.; Lerondel, G.; Grand, J.; Kostcheev, S.; Billot, L.; Vial, A.; Bachelot, R.; Royer, P.; Chang, S. Near-Field Photochemical Imaging of Noble Metal Nanostructures. *Nano Lett.* **2005**, *5*, 615−619.

(24) Hubert, C.; Bachelot, R.; Plain, J.; Kostcheev, S.; Lerondel, G.; Juan, M.; Royer, P.; Zou, S.; Schatz, G. C.; Wiederrecht, G. P. Near-Field Polarization Effects in Molecular-Motion-Induced Photochemical Imaging. *J. Phys. Chem. C* **2008**, *112*, 4111−4116.

(25) Hubert, C.; Fiorini-Debuisschert, C.; Maurin, I.; Nunzi, J.-M.; Raimond, P. Spontaneous Patterning of Hexagonal Structures in an Azo-Polymer Using Light-Controlled Mass Transport. *Adv. Mater.* **2002**, *14*, 729−732.

(26) Murray-Méthot, M.-P. M., N.; Masson, J.-F. Analytical and Physical Optimization of Nano-Hole Array Sensors Prepared by Modified Nanosphere Lithography. *Analyst* **2008**, *133*, 1714−1721.

(27) Guieu, V.; Lagugné-Labarthet, F.; Servant, L.; Talaga, D.; Sojic, N. Ultrasharp Optical-Fiber Nanoprobe Array for Raman Local-Enhancement Imaging. *Small* **2008**, *4*, 96−99.

(28) Li, J. F.; Huang, Y. F.; Ding, Y.; Yang, Z. L.; Li, S. B.; Zhou, X. S.; Fan, F. R.; Zhang, W.; Zhou, Z. Y.; Wu, D. Y.; Ren, B.; Wang, Z. L.; Tian, Z. Q. Shell-Isolated Nanoparticle-Enhanced Raman Spectroscopy. *Nature* **2010**, *464*, 392−395.

(29) Chung, P.-Y.; Lin, T.-H.; Schultz, G.; Batich, C.; Jiang, P. Nanopyramid Surface Plasmon Resonance Sensors. *Appl. Phys. Lett.* **2010**, *96*, 261108.

(30) Lin, T.-H.; Linn, N. C.; Tarajano, L.; Jiang, B.; Jiang, P. Electrochemical SERS at Periodic Metallic Nanopyramid Arrays. *J. Phys Chem. C* **2009**, *113*, 1367−1372.

(31) Sun, C.-H.; Linn, N. C.; Jiang, P. Templated Fabrication of Periodic Metallic Nanopyramid Arrays. *Chem. Mater.* **2007**, *19*, 4551−4556.

(32) Stoerzinger, K. A.; Hasan, W.; Lin, J. Y.; Robles, A.; Odom, T. W. Screening Nanopyramid Assemblies to Optimize Surface Enhanced Raman Scattering. *J. Phys. Chem. Lett.* **2010**, *1*, 1046−1050.

(33) Alexander, T. A. Applications of Surface-Enhanced Raman Spectroscopy (SERS) for Biosensing: An Analysis of Reproducible,

Commercially Available Substrates. *Proc. SPIE—Int. Soc. Opt. Eng.* **2005**, *6007*, 600703.

(34) Hartschuh, A. Tip-Enhanced Near-Field Optical Microscopy. *Angew. Chem., Int. Ed.* **2008**, *47*, 8178−8191.

(35) Cançado, L. G.; Jorio, A.; Ismach, A.; Joselevich, E.; Hartschuh, A.; Novotny, L. Mechanism of Near-Field Raman Enhancement in One-Dimensional Systems. *Phys. Rev. Lett.* **2009**, *103*, 186101.

(36) Schatz, G. C.; Young, M. A.; Van Duyne, R. P. In *Surface-Enhanced Raman Scattering*; Kneipp, K., Moskovits, M., Kneipp, H., Eds.; Springer-Verlag: Berlin, 2006; Vol. *103*, p 19−46.

(37) Schaller, R. D.; Saykally, R. J.; Shen, Y. R.; Lagugné-Labarthet, F. Poled Polymer Thin-Film Gratings Studied with Far-Field Optical Diffraction and Second-Harmonic Near-Field Microscopy. *Opt. Lett.* **2003**, *28*, 1296−1298.

(38) Viswanatahan, N. K.; Balasubramanian, S.; Li, L.; Tripathy, S. K.; Kumar, J. A Detailed Investigation of the Polarization-Dependent Surface-Relief-Grating Formation Process on Azo Polymer Films. *Jpn. J. Appl. Phys.* **1999**, *38*, 5928−5937.

(39) Lefin, P.; Fiorini, C.; Nunzi, J. M. Anisotropy of the Photo-Induced Translation Diffusion of Azobenzene Dyes in Polymer Matrices. *Pure Appl. Opt.* **1998**, *7*, 71−82.

(40) Kim, K.; Lee, Y. M.; Lee, H. B.; Park, Y.; Bae, T. Y.; Jung, Y. M.; Choi, C. H.; Shin, K. S. Visible Laser−Induced Photoreduction of Silver 4-Nitrobenzenethiolate Revealed by Raman Scattering Spectroscopy. *J. Raman Spectrosc.* **2010**, *41*, 187−192.

(41) Kim, K.; Lee, I.; Lee, S. J. Photolytic Reduction of 4-Nitrobenzenethiol on Au Mediated via Ag Nanoparticles. *Chem. Phys. Lett.* **2003**, *377*, 201−204.

(42) Sun, S.; Birke, R. L.; Lombardi, J. R.; Leung, K. P.; Genack, A. Z. Photolysis of p-Nitrobenzoic Acid on Roughened Silver Surfaces. *J. Phys. Chem.* **1988**, *92*, 5965−5972.

(43) van Schrojenstein Lantman, E. M.; Deckert-Gaudig, T.; Mank, A. J. G.; Deckerts, V.; Weckhuysen, B. M. Catalytic Processes Monitored at the Nanoscale with TERS. *Nat. Nanotechnol.* **2012**, *7*, 583−586.